Ultraluminous X-ray sources out toz~ 0.3 in the COSMOS field

07 June 2023

A&A 514, A85 (2010)
DOI: 10.1051/0004-6361/200912544

Astronomy & Astrophysics

Ultraluminous X-ray sources out to $z \sim 0.3$ in the COSMOS field

V. Mainieri[1], C. Vignali[2,3], A. Merloni[4,5], F. Civano[6], S. Puccetti[7], M. Brusa[5], R. Gilli[3], M. Bolzonella[3], A. Comastri[3], G. Zamorani[3], M. Aller[9], M. Carollo[9], C. Scarlata[9,10], M. Elvis[6], T. L. Aldcroft[6], N. Cappelluti[5], G. Fabbiano[6], A. Finoguenov[5], F. Fiore[8], A. Fruscione[6], A. M. Koekemoer[11], T. Contini[12], J.-P. Kneib[13], O. Le Fèvre[13], S. Lilly[9], A. Renzini[14], M. Scodeggio[15], S. Bardelli[3], A. Bongiorno[5], K. Caputi[9], G. Coppa[3], O. Cucciati[16], S. de la Torre[13], L. de Ravel[13], P. Franzetti[15], B. Garilli[15], A. Iovino[16], P. Kampczyk[9], C. Knobel[9], K. Kovač[9], F. Lamareille[12], J.-F. Le Borgne[12], V. Le Brun[13], C. Maier[9], M. Mignoli[3], R. Pello[12], Y. Peng[9], E. Perez Montero[12], E. Ricciardelli[17], J. D. Silverman[9], M. Tanaka[1], L. Tasca[13], L. Tresse[13], D. Vergani[3], E. Zucca[3], P. Capak[19], O. Ilbert[13], C. Impey[18], M. Salvato[19], N. Scoville[19], Y. Taniguchi[20], and J. Trump[18]

[1] ESO, Karl-Schwarzschild-Strasse 2, 85748 Garching bei München, Germany
e-mail: vmainier@eso.org
[2] Dipartimento di Astronomia, Università degli Studi di Bologna, via Ranzani 1, 40127 Bologna, Italy
[3] INAF - Osservatorio Astronomico di Bologna, via Ranzani 1, 40127 Bologna, Italy
[4] Excellence Cluster Universe, TUM, Boltzmannstr. 2, 85748 Garching bei München, Germany
[5] Max-Planck-Institute für Extraterrestrische Physik, Postfach 1312, 85741, Garching bei München, Germany
[6] Harvard-Smithsonian Center for Astrophysics, 60 Garden St., Cambridge, MA 02138, USA
[7] ASI Science Data Center, via Galileo Galilei, 00044 Frascati Italy
[8] INAF - Osservatorio astronomico di Roma, via Frascati 33, 00040 Monteporzio Catone, Italy
[9] Institute of Astronomy, Swiss Federal Institute of Technology (ETH Hönggerberg), 8093, Zürich, Switzerland
[10] Spitzer Science Center, Pasadena, CA, 91125, USA
[11] Space Telescope Science Institute, Baltimore, Maryland 21218, USA
[12] Laboratoire d'Astrophysique de Toulouse-Tarbes, Université de Toulouse, CNRS, 14 avenue Edouard Belin, 31400 Toulouse, France
[13] Laboratoire d'Astrophysique de Marseille, Marseille, France
[14] INAF - Osservatorio astronomico di Padova, Vicolo Dell'Osservatorio 5, 35122 Padova, Italy
[15] INAF - IASF Milano, Milan, Italy
[16] INAF Osservatorio Astronomico di Brera, Milan, Italy
[17] Dipartimento di Astronomia, Universita di Padova, Padova, Italy
[18] Steward Observatory, University of Arizona, 933 North Cherry Avenue, Tucson, AZ 85721, USA
[19] California Institute of Technology, MC 105-24, 1200 East California Boulevard, Pasadena, CA 91125, USA
[20] Research Center for Space and Cosmic Evolution, Ehime University, Bunkyo-cho 2-5, Matsuyama 790-8577, Japan

Received 20 May 2009 / Accepted 22 February 2010

ABSTRACT

Context. Using Chandra observations we identified a sample of seven off-nuclear X-ray sources in the redshift range $z = 0.072-0.283$, located within optically bright galaxies in the COSMOS Survey. All of them, if associated with their closest bright galaxy, would have $L[0.5-7\ \mathrm{keV}] > 10^{39}$ erg s^{-1} and therefore can be classified as ultraluminous X-ray sources (ULXs).
Aims. Using the multi-wavelength coverage available in the COSMOS field, we studied the properties of the host galaxies of these ULXs. In detail, we derived their star formation rate from Hα measurements and their stellar masses using SED fitting techniques with the aim to compute the probability to have an off-nuclear source based on the host galaxy properties. We divided the host galaxies in different morphological classes with the available ACS/HST imaging.
Methods. We selected off-nuclear candidates with the following criteria: 1) the distance between the X-ray and the optical centroid has to be larger than 0.9″, larger than 1.8 times the radius of the Chandra positional error circle and smaller than the Petrosian radius of the host galaxy; 2) the optical counterpart is a bright galaxy ($R_{\mathrm{AB}} < 22$); 3) the redshift of the counterpart is lower than $z = 0.3$; 4) the source has been observed in at least one Chandra pointing at an off-axis angle smaller than 5′; 5) the X-ray positional error is smaller than 0.8″. We verified each candidate super-imposing the X-ray contours on the optical/IR images. We expect less than one misidentified AGN due to astrometric errors and on average 1.3 serendipitous background source matches.
Results. We find that our ULXs candidates are located in regions of the SFR versus $M_\star$ plane where one or more off-nuclear detectable sources are expected. From a morphological analysis of the ACS imaging and the use of rest-frame colours, we find that our ULXs are hosted both in late and early type galaxies. Finally, we find that the fraction of galaxies hosting a ULX ranges from ≈0.5% to ≈0.2% going from $L_{0.5-2\ \mathrm{keV}} = 3 \times 10^{39}$ erg s^{-1} to $L_{0.5-2\ \mathrm{keV}} = 2 \times 10^{40}$ erg s^{-1}.

Key words. X-rays: galaxies – X-rays: binaries – X-rays: general – surveys

1. Introduction

An intriguing class of X-ray objects are the so called ultraluminous X-ray sources (ULXs). Here an ULX is defined as an X-ray source in an extra-nuclear region of a galaxy with an observed luminosity in excess of 10^{39} erg s^{-1} in the 0.5–7 keV band. These X-ray luminosities are higher than expected for spherical Eddington-limited accretion onto a ∼10 $M_\odot$ black hole. ULXs

were known already from studies with Einstein, ROSAT, and ASCA (e.g. Fabbiano 1989; Colbert & Ptak 2002; Makishima et al. 2000), but it was after the advent of Chandra with its combination of high angular resolution and moderate spectral resolution that it has been possible to make significant progress in their study (e.g. Roberts et al. 2004; Swartz et al. 2004). There is a wide debate in the literature on the nature of these sources. They may be powered by accretion onto stellar-mass black holes assuming that there is relativistic beaming (e.g. Körding et al. 2002), or radiative anisotropy (e.g. King 2002), or they may be associated with super-Eddington disks (e.g. Begelman 2002). It has also been suggested that ULXs represent a new class of intermediate-mass (10^2–10^5 $M_\odot$) black holes (e.g. Colbert & Mushotzky 1999; Miller & Colbert 2004). These intermediate-mass black holes may be fed by Roche lobe overflow from a tidal captured stellar companion that is not destroyed by tidal heating (Hopman et al. 2004). Off-nuclear AGN activity could also be a signature of a recoiling massive black hole: a massive black hole binary coalesces and causes gravitational waves which can give a kick to the center of mass of the system. If the recoiling black hole retains the inner parts of its accretion disk, we could see its luminous phase as an off-nuclear AGN (see Volonteri & Madau 2008, and references therein). Finally, ULXs could also be the high-luminosity extension of supernovae (e.g. Swartz et al. 2004).

Many of the previous studies based on Chandra data are focused on local galaxies, where the Chandra angular resolution allows the detection of several off-nuclear sources in one single galaxy. In this paper, we select a sample of ULXs from the Chandra survey in the COSMOS field. We have here the advantage to combine deep X-ray observation with a wealth of multi-wavelength ancillary data that we will use to put constraints on the nature of these sources and on the properties of their host galaxies. The redshift range that we cover is up to $z \simeq 0.3$. A study of off-nuclear sources in a similar redshift range was performed by Lehmer et al. (2006) on the Chandra Deep Fields (CDFs).

We quote in this paper magnitudes in the AB system and assume a cosmology with $H_0 = 70\ \mathrm{km\,s^{-1}\,Mpc^{-1}}$, $\Omega_\mathrm{M} = 0.3$ and $\Omega_\Lambda = 0.7$.

2. Sample selection

We have selected off-nuclear X-ray candidates from the Chandra COSMOS Survey (C-COSMOS), which is a recently completed 1.8 Ms Chandra program to image the central 0.9 deg^2 of the COSMOS field with an effective exposure ranging from ~160 ks to ~80 ks going from the center to the borders of the field (Elvis et al. 2009). The limiting source detection depths are 1.9×10^{-16} erg cm^{-2} s^{-1} in the [0.5–2 keV] band, 7.3×10^{-16} erg cm^{-2} s^{-1} in the [2–10 keV] band, and 5.7×10^{-16} erg cm^{-2} s^{-1} in the [0.5–10 keV] band. We used a point source catalog including 1761 objects detected in at least one band (0.5–2, 2–7 and 0.5–7 keV) with a maximum likelihood ratio larger than detml = 10.8, corresponding to a probability of $\sim 2 \times 10^{-5}$ that a catalog source is instead a background fluctuation (Puccetti et al. 2009). The optical and infrared identifications of almost all (99.7%) of the sources are reported in Civano et al. (2010, in prep.)[1].

As a first step to select off-nuclear X-ray sources, we verified the X-ray position accuracy that we have in the C-COSMOS observations following the procedure presented in Sect. 4.3 of Puccetti et al. (2009). A set of 49 Chandra ACIS-I pointings has been simulated with the MARX[2] simulator, adopting the same exposure times, aim points, and roll-angles as the real C-COSMOS pointings. The detection code PWDetect (Damiani et al. 1997) was applied to the simulated data. We then compared the output of the detection algorithm with the input catalog of the simulation. In Fig. 1 we show the distribution of the difference between the detection algorithm positions and the input positions in units of the X-ray positional error. The last was estimated as the ratio of the PSF at the position of the source and the square root of the net background subtracted source counts. In comparison with Fig. 10 of Puccetti et al. (2009), we restricted the analysis only to sources that were detected at least in one image at an off-axis angle smaller than 5′ to take advantage of an excellent PSF. From the distribution in Fig. 1, we find that 94% of the sources have offsets below 1.8 times the positional error. We will adopt this value as a threshold to select off-nuclear candidates and therefore we expect that up to 6% of our sample is contaminated by nuclear X-ray sources with large astrometric errors. We will shortly come back to this issue. Another possible source of spurious off-nuclear objects could be a poor astrometric accuracy of the X-ray images. According to Fig. 6 of Elvis et al. (2009), 95% of the Chandra sources have an absolute astrometric accuracy better than 1.4″. For our study we aim at even better astrometric accuracy, therefore we considered only the X-ray sources with an X-ray positional error smaller that 0.8″. We show the comparison between X-ray coordinates and optical coordinates for sources with a secure identification in Fig. 2: 95% of the X-ray sources have an absolute astrometric accuracy better than 0.9″.

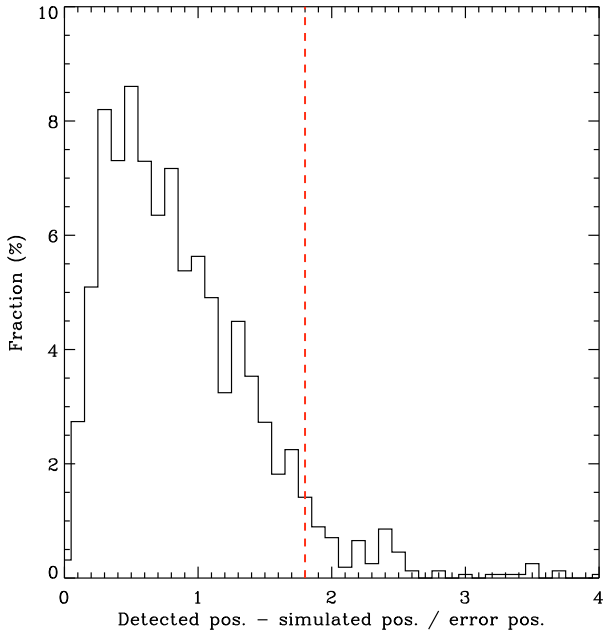

Fig. 1. Distribution of the difference between the detected X-ray positions and the input positions in units of the X-ray positional error.

Summarizing, the off-nuclear candidates were selected with the following criteria:

a) The distance between the X-ray centroid and the optical centroid has to be larger than 1.8 times the radius of the Chandra positional error circle at that position.

[1] The ULX candidates presented in this paper are flagged as "off-nuclear" sources in Civano et al. (2010, in prep.).

[2] http://space.mit.edu/CXC/MARX.

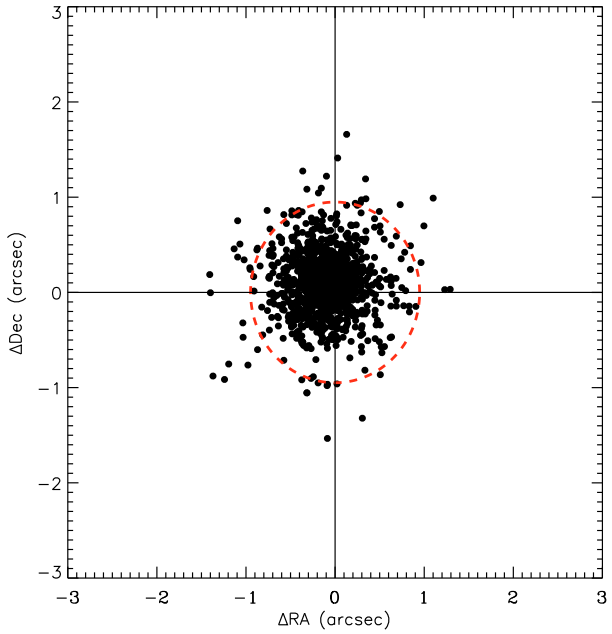

Fig. 2. X-ray to optical offsets in arcsec for X-ray sources with a secure identification (Civano et al. 2010, in prep.) and with an X-ray positional error smaller than 0.8″. The circle of 0.9″ radius encompasses 95% of the X-ray sources.

b) The X-ray positional error is smaller than 0.8″.
c) The source was observed in at least one Chandra pointing at an off-axis angle smaller than 5′.
d) The optical counterpart is a bright galaxy ($R_{AB} < 22$).
e) The redshift of the host galaxy is less than $z = 0.3$. The projected linear distance corresponding to an average Chandra positional error is ∼4 kpc at $z = 0.3$. This means we will consider only off-nuclear candidates that are more than ∼7 kpc away from the center of the galaxy at $z = 0.3$. At larger redshifts we would be able to select only off-nuclear candidates that are at larger distances (>7 kpc) from the host galaxy center, where the number of observed off-nuclear sources seems to decrease (Swartz et al. 2004) and we would be more affected by the contamination of background objects. Therefore we limit our sample to $z < 0.3$.
f) The distance between the X-ray centroid and the optical centroid is larger than 0.9″and smaller than the Petrosian radius (Petrosian 1976, R_P[3]) of the galaxy, which we use as a measure of the galaxy's extension.

If we consider the selection criteria b)–e), only sixteen sources from the C-COSMOS catalog satisfy all of them. Based on our previous discussion of Fig. 1 we expect up to 6% of our sample to be due to nuclear X-ray sources with large astrometric errors, therefore we can conclude that our sample of ULXs contains less than one misidentified AGN.

For all the candidates provided by these selection criteria we verified that no other counterpart closer to the Chandra position was present in any band from the u^* ($\lambda_{center} = 374.3$ nm) filter to 24 micron. After this one-by-one check, we were left with seven off-nuclear source candidates. Cutouts of these objects, obtained from the COSMOS HST/ACS F814W imaging (Koekemoer et al. 2007), are shown in Fig. 3, together with the corresponding Chandra [0.5−7 keV] image.

Each of our off-nuclear sources has an estimate of the X-ray flux in the [0.5−7] keV band reported in Elvis et al. (2009). These fluxes are derived from the counts estimated by EMLdetect[5], corrected to an area including 90% of the PSF (Puccetti et al. 2009). In some cases such an area is large enough to include the whole host galaxy and therefore the X-ray flux could be the total integrated flux of the host galaxy itself. This would include the contribution from the population of X-ray binaries in the host, emission from diffuse gas and a possible weak central AGN. In order to estimate these possible contaminations on the measured X-ray fluxes, we performed aperture photometry for each off-nuclear source. The radii of the apertures were chosen with increasing size from a minimum of 1″ up to include the whole galaxy. In Fig. 4, we plot the net counts in the [0.5−7] keV band as a function of the aperture radius. For four of our sources (XID = 2418, 3441, 11100, 11938) the counts measured at different apertures are constant within the uncertainties. Therefore, we assume that the contribution of the host galaxy is not significant compared with the uncertainties on the measure. For the remaining three sources (XID = 1151, 1388, 1870) the counts rise with the aperture radius and there may be a significant contamination due to the integrated flux of the whole galaxy. In order to minimize this contamination, we considered the measured counts in the smaller aperture (1″). We then used the known PSF shape at the position of the source to estimate the expected fraction between the counts measured in an aperture of 1″and those over an area corresponding to 90% of the PSF. We then used this ratio to convert our measured counts on the 1″aperture into the expected ones on a 90% PSF area. These corrected counts are indicated with a filled circle in the plots of Fig. 4, and we used them to estimate the X-ray fluxes.

Full band 0.5−7 keV fluxes and errors were computed converting counts rates to fluxes with the formula Flux = $B_{rate}/(CF \star 10^{11})$, where B_{rate} is the count rate estimated as described above, and CF is the energy conversion factor. This conversion factor varies with the energy band and the spectral index Γ assumed for the power-law spectrum. We used the correction factor CF = 0.89 counts erg^{-1} cm^2 reported in Table 4 of Elvis et al. (2009) obtained for the 0.5−7 keV band and Γ = 1.7. We decided for this average value of the spectral index following the study of Swartz et al. (2004) that has found a mean power-law index of $\Gamma = 1.74 \pm 0.03$ for a sample of 154 ULX candidates observed with Chandra. We finally report in Table 1 the 0.5−7 keV luminosities and errors for the seven off-nuclear sources. All sources have luminosities well in excess of 10^{39} erg s^{-1} in the 0.5−7 keV band (the lowest X-ray luminosity in this band is $\approx 9 \times 10^{39}$ erg s^{-1}) and are therefore classified as ULX sources, using either spectroscopic or photometric redshifts.

We have secure spectroscopic redshifts for four host galaxies from zCOSMOS VIMOS observations at VLT (Lilly et al. 2007, 2009). For the remaining three objects we used the extremely accurate photometric redshifts available in the COSMOS field (Ilbert et al. 2009; Salvato et al. 2009) based on 30 broad, intermediate, and narrow bands from the UV to the mid-IR. We show in Fig. 5 the X-ray luminosity in the [0.5−7] keV band versus redshift of the seven ULXs. The X-ray luminosities were computed according to the formula

$$L_X = 4\pi d_L^2 f_X (1+z)^{\Gamma-2}, \quad (1)$$

[3] R_P is defined as the radius at which the ratio (r_P) of the local surface brightness at that radius and the mean surface brightness within that radius equals some specified value $r_{P,lim}$. For a surface brightness distribution described by a de Vaucouleurs or an exponential profile, a value $r_{P,lim} = 0.2$ is reached at $R_P \sim 1.8\, R_{1/2}$ and $R_P \sim 2.2\, R_{1/2}$, respectively ($R_{1/2}$ is the half-light radius of the galaxy, see Fig. 17 of Scarlata et al. 2007).

[5] http://xmm.esac.esa.int/sas/8.0.0/emldetect

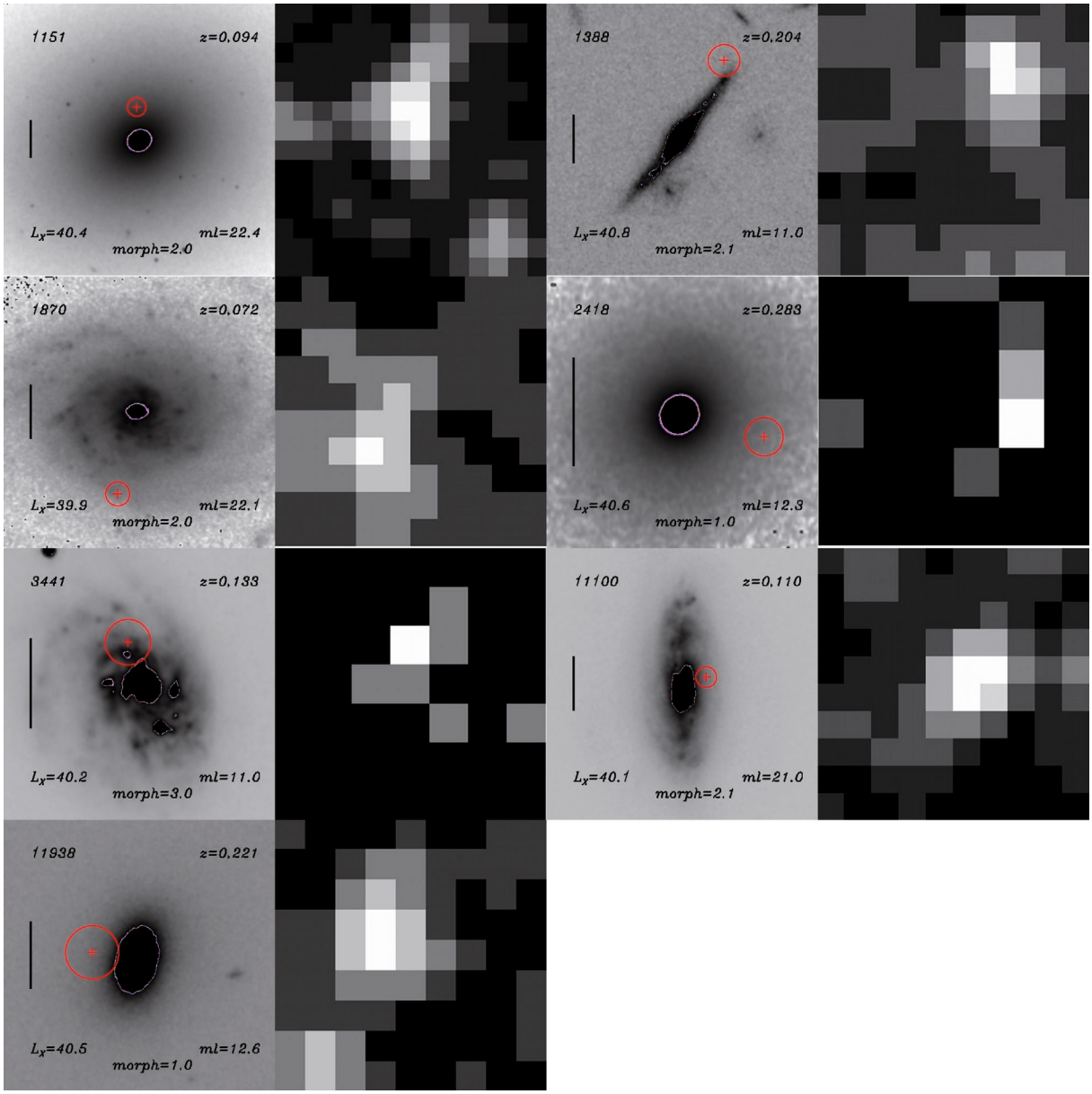

Fig. 3. Cutouts in the HST/ACS F814W band (Koekemoer et al. 2007) of the seven X-ray off-nuclear sources in the C-COSMOS field. The red cross indicates the position of the X-ray centroid and the red circle the X-ray positional error (Elvis et al. 2009). We provide for each object the Chandra ID (*top-left*), the redshift (*top-right*), the logarithm of the X-ray luminosity in the [0.5−7] keV band (*bottom-left*), the maximum likelihood ratio for the X-ray detection (*bottom-right*), the morphological classification of the host galaxy (bottom-middle; see Sect. 3.1). The images have different sizes for display purposes; the vertical bar in each cutout corresponds to 2″ . On the right of each ACS cutout is the corresponding Chandra [0.5−7 keV] image.

where $d_{\rm L}$ is the luminosity distance, $f_{\rm X}$ is the X-ray flux in the [0.5−7] keV band, and Γ is the X-ray photon index. We assumed $\Gamma = 1.7$ (see discussion in this section). Different symbols correspond to the morphological classes of the host galaxies (see Sect. 3.1). Squares are the off-nuclear sources from Lehmer et al. (2006); crosses are the collection of local ULXs by Liu & Mirabel (2005). The dashed line corresponds to the flux limit of the C-COSMOS survey, $S_{\rm lim}[0.5-7] = 4.7 \times 10^{-16}$ erg cm^{-2} s^{-1}.

In order to estimate how many background sources we expect to contaminate our sample, we applied a random shift between 30″ and 2′ to the C-COSMOS sources and searched for chance coincidences with $R_{\rm AB} < 22$ and $z < 0.3$ galaxies. We repeated this procedure 10,000 times and found that on average the chance coincidences are ≈1.3. Only for 2% of the 10 000 simulations we found more than three chance coincidences. Summarizing, we expect less than one misidentified AGN due to astrometric errors and on average 1.3 serendipitous background source matches.

3. Host galaxy properties

3.1. Galaxy classification

Studies of local samples of ULXs (e.g. Swartz et al. 2004) have shown that these sources are mainly present in late type galaxies. A visual inspection of Fig. 3 suggests that the ULXs at intermediate redshifts that we are studying are hosted in both early and late type galaxies (ETGs and LTGs, hereafter).

To confirm this impression we classified the host galaxies based on their morphology and colors (e.g. Mignoli et al. 2009).

Table 1. Properties of ULXs in C-COSMOS.

XID[a]	RA	Dec	Counts[b]	log L_X[c]	Pos. error[d]	Offset	Offset	Offset[e]	Off-axis[f]
	(J2000)[4]		(0.5−7 keV)	(erg s^{-1})	(arcsec)	(arcsec)	(kpc)		(arcmin)
1151	10:00:10.39	02:09:23.40	28	$40.4^{40.5}_{40.1}$	0.5	1.67	2.91	3.42	2.8
1388	10:01:08.46	02:01:06.05	17	$40.8^{40.9}_{40.4}$	0.6	3.62	12.12	5.73	2.6
1870	10:01:03.76	02:30:50.22	9	$39.9^{40.2}_{39.3}$	0.4	3.12	4.66	7.25	2.6
2418	10:00:08.43	02:14:47.65	6	$40.6^{40.8}_{40.1}$	0.3	1.58	6.76	4.53	1.3
3441	09:59:33.78	01:49:06.92	5	$40.2^{40.5}_{39.8}$	0.5	0.95	2.26	1.87	3.7
11 100	10:00:58.65	02:11:39.90	12	$40.1^{40.3}_{39.9}$	0.4	0.92	1.85	2.37	3.4
11 938	10:00:43.02	02:00:32.74	7	$40.5^{40.7}_{40.2}$	0.8	1.39	4.79	1.77	4.4

Notes. [(a)] ID of the Chandra source (Elvis et al. 2009) . [(b)] X-ray counts in the [0.5−7] keV band. [(c)] Logarithm of the [0.5−7] keV X-ray luminosity. [(d)] X-ray positional error. [(e)] Ratio of the distance between the X-ray centroid and the optical centroid over the radius of the Chandra positional error circle. [(f)] Off-axis angle value in the image where the source is closer to the on-axis position.

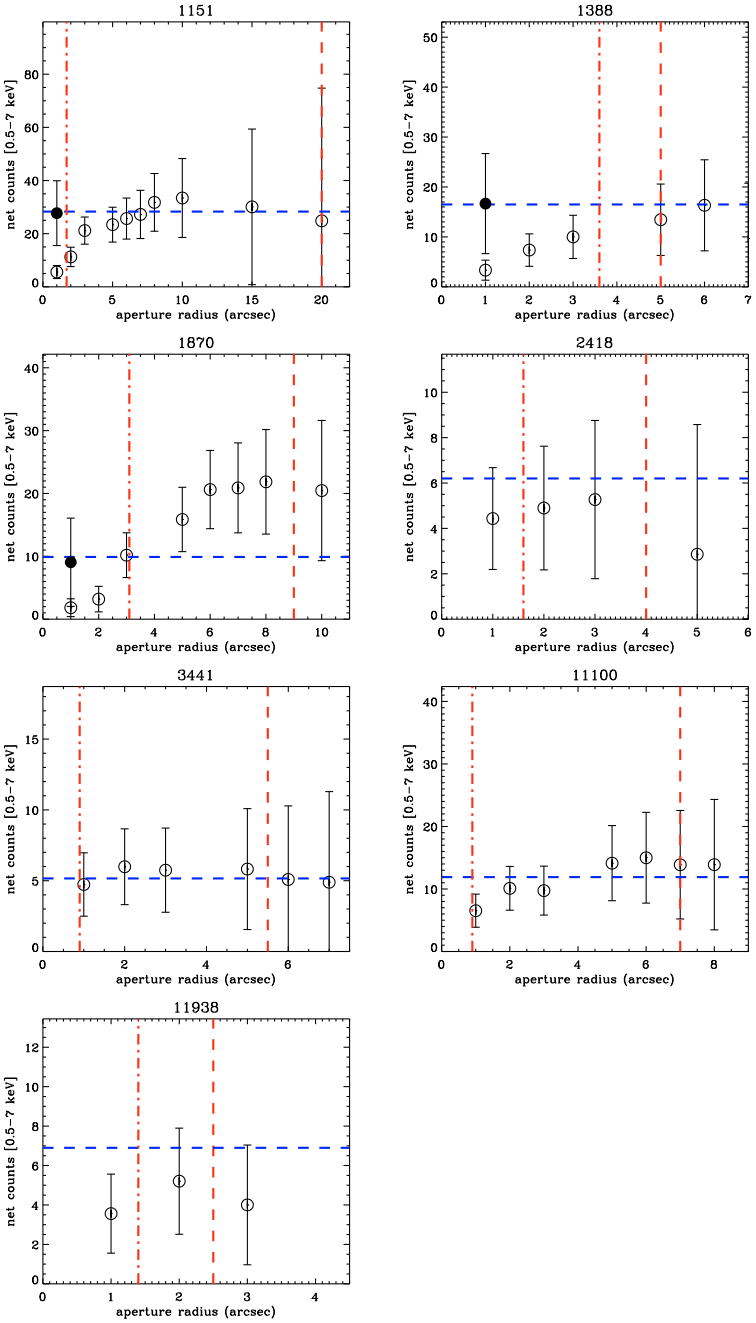

Fig. 4. Aperture photometry for each off-nuclear candidate. The vertical dot-dashed line indicates the distance between the X-ray position and the centroid of the host galaxy; the vertical dashed line is the Petrosian radius of the host galaxy; the horizontal line corresponds to the counts estimated by EMLdetect (Puccetti et al. 2009). For objects XID = 1151, 1388, and 1870, the filled circles represent the photometry on an area including 90% of the PSF obtained applying an aperture correction factor to the photometry measured on an aperture of 1″ radius (see discussion in Sect. 2).

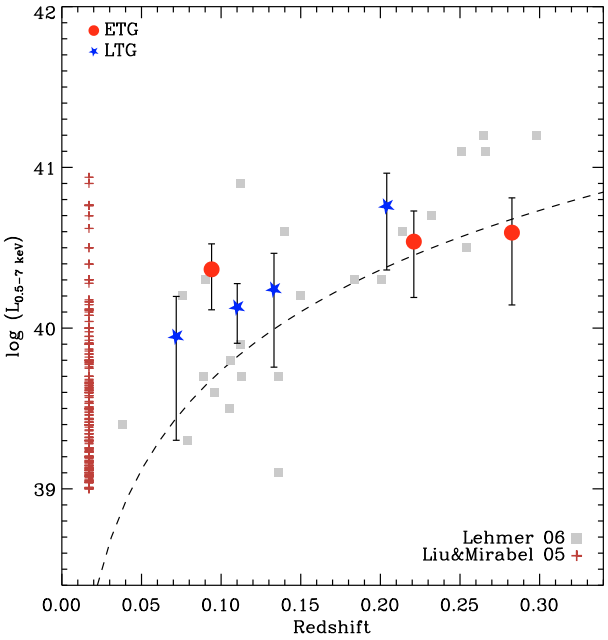

Fig. 5. X-ray luminosity in the 0.5−7 keV band vs. redshift of the seven off-nuclear sources. The different symbols correspond to the host galaxy classification based on morphology and rest-frame colors: circles are ETGs, while stars are LTGs (see Sect. 3.1). Squares are the off-nuclear sources from Lehmer et al. (2006); crosses are the collection of local off-nuclear sources by Liu & Mirabel (2005). The dashed line corresponds to the flux limit in the deepest region of the C-COSMOS survey: $S_{lim}[0.5–7] = 4.7 \times 10^{-16}$ cgs.

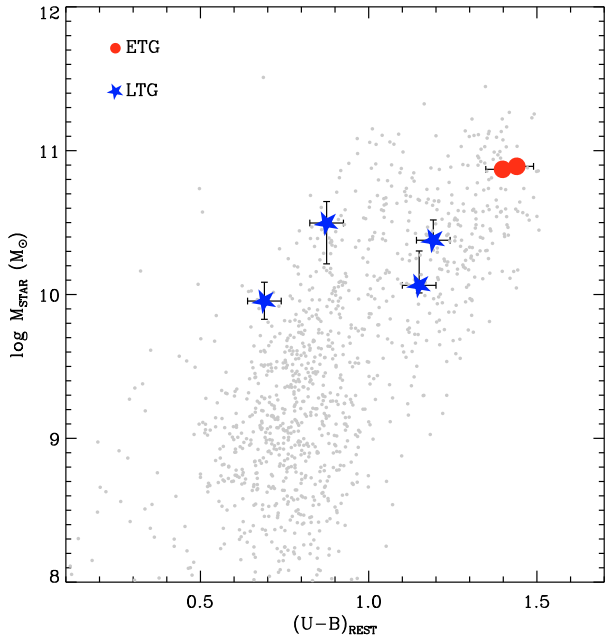

Fig. 6. Color-mass diagram: circles and stars are respectively ULX host galaxies classified as ETGs and LTGs based on their morphology/colors; the dots are galaxies in the C-COSMOS area with $z < 0.3$ and $R_{AB} < 22$. For the source XID = 1151 the photometric coverage is limited to few bands and we cannot constrain its stellar mass.

Taking advantage of the COSMOS HST/ACS F814W images (Koekemoer et al. 2007), we used an accurate morphological classification derived by Scarlata et al. (2007) through the Zurich Estimator of Structural Type (ZEST). Scarlata et al. (2007) describe in detail the methodology and the performances of this method. We only recall here that the ZEST classification is based on a) five non-parametric diagnostics (asymmetry A, concentration C, Gini coefficient G, 2nd order moment of the brightest 20% of galaxy pixels M_{20}, ellipticity ϵ); and b) the exponent n of single Sersic fits to the two-dimensional surface brightness distributions. ZEST assigns to each galaxy a morphological type (1 = early type; 2 = disk; 3 = irregular) and a bulgeness parameter that splits the disk galaxies in four separate bins, from bulge dominated disks (2.0) to pure disk galaxies (2.3). For the bulge-dominated galaxies (2.0), we complemented the morphological information with their rest-frame colors to further subdivide them: if they have red $U - B$ rest-frame colors, we included them in the ETGs sample (XID = 1151), otherwise we classified them as LTGs (XID = 1870). In Fig. 6 we plot the color-mass diagram for our ULX host galaxies: they can be divided into three ETGs and four LTGs. We will describe in Sect. 3.2 the method used to estimate stellar masses.

The slight preference for ULXs to be hosted in LTGs could be explained by the different shapes of the X-ray luminosity function (XLF) for Low-Mass X-ray Binaries (LMXBs) and High-Mass X-ray Binaries (HMXBs) derived for local galaxies (Grimm et al. 2003; Gilfanov 2004): the former has an abrupt cut-off at $L_X \approx 10^{39}$ erg s^{-1}, while the latter can be described with a power-law with a slope $\alpha = 1/6$. Because early-type stars are the dominant stellar population of LTGs, we expect X-ray binaries with O or B type companions, HMXBs, to be common in these objects. This translates into a higher chance to detect ULXs in LTGs or, in any case, in galaxies with current star formation activity.

3.2. Stellar masses and star formation rates.

Stellar masses ($M_\star$) are derived from the stellar population synthesis model that represents the best fit to the observed photometry (from the u^* band to 4.5 μm) using a χ^2 minimization technique. The procedure is explained in detail by Bolzonella et al. (2009). Here we only recall the basic ingredients of the Spectral Energy Distribution (SED) fitting procedure:

- stellar population synthesis models from the libraries of Bruzual & Charlot (2003);
- eleven "smooth" star formation histories for each library: one constant star formation model plus 10 τ-model with e-folding time-scales τ = 0.1, 0.3, 0.6, 1, 2, 3, 5, 10, 15, 30 Gyr;
- a Chabrier initial mass function;
- a Calzetti extinction law with $0 < A_V < 3$;
- solar metalicity ($Z = Z_\odot$).

The star formation rate (SFR) values were estimated using when possible (for three ULXs) the Hα λ6563 line flux as measured by the routine Platefit (Lamareille et al. 2009, in prep.), with a correction for reddening. We used the Kennicutt (1998) relation between Hα and SFR: $\mathrm{SFR}(M_\odot\ \mathrm{yr}^{-1}) = (7.9\times10^{-42})L(H\alpha)\ \mathrm{erg\ s}^{-1}$. The de-reddened flux of Hα was computed according to the formula $F_{\rm der} = F_{\rm obs} \times 10^{c[1+f(\lambda)]}$ where $f(\lambda) = 3.15854 \times 10^{-1.02109\lambda} - 1$ and $c = 1.47E_{B-V}$ (Seaton 1979; Maier et al. 2005). If a measure of the $H\beta$ flux was available we estimated E_{B-V} from the Balmer decrement, adopting the O'Donnell (1994) Milky Way extinction curve. Otherwise, we used the average value $\langle E_{B-V}\rangle \sim 0.2$ mag derived by Moustakas et al. (2006). For the sources without $H\alpha$ in the spectral range or for

those where we have only a photometric redshift, we used the SFR estimate from the SED fitting procedure.

From the COSMOS catalog (Capak et al. 2007; Ilbert et al. 2009) we selected a comparison sample of galaxies inside the area covered by Chandra. We imposed the same constraints used to select the off-nuclear candidates: $z < 0.3$ and $R_{AB} < 22$. We also removed all sources that are best fitted by stellar SED templates (Ilbert et al. 2009). At the end, the comparison sample consists of 2066 galaxies. For all of them we derived stellar masses and SFR values as described above.

We now estimate the probability to have an off-nuclear source given a host galaxy with a particular stellar mass and SFR. We will consider both LMXBs and HMXBs.

For LMXBs we used the average XLF derived by Gilfanov (2004). This is described by a power-law with two breaks, from their Eq. (8):

$$\frac{\mathrm{d}N}{\mathrm{d}L_{38}} = \begin{cases} K_1 \left(L_{38}/L_{b,1}\right)^{-\alpha_1} & L_{38} < L_{b,1} \\ K_2 \left(L_{38}/L_{b,2}\right)^{-\alpha_2} & L_{b,1} < L_{38} < L_{b,2} \\ K_3 \left(L_{38}/L_{\rm cut}\right)^{-\alpha_3} & L_{b,2} < L_{38} < L_{\rm cut} \\ 0 & L_{38} > L_{\rm cut}, \end{cases} \quad (2)$$

where $L_{38} = L_{\rm X}/10^{38}$ erg/s and normalizations $K_{1,2,3}$ are defined as

$$K_2 = K_1 \left(L_{b,1}/L_{b,2}\right)^{\alpha_2}$$
$$K_3 = K_2 \left(L_{b,2}/L_{\rm cut}\right)^{\alpha_3}.$$

We used the best-fitting parameter derived by Gilfanov (2004): $\alpha_1 = 1.0$, $L_{b,1} = 0.19$, $\alpha_2 = 1.86$, $L_{b,2} = 5.0$, $\alpha_3 = 4.8$. The high-luminosity cut-off was fixed at $L_{\rm cut} = 500$. For the average normalization we used the best-fitting value given by Gilfanov (2004), $K_1 = 440.4 \pm 25.9$ per 10^{11} $M_\odot$, and we will assume a linear relation between the number of X-ray sources and stellar mass as found by the same authors (see Sec. 5 of Gilfanov 2004). We note that up to $L_{\rm X} \approx 2 \times 10^{39}$ erg s^{-1} the XLF of Gilfanov (2004) is consistent with later studies (e.g. see Fig. 14 of Humphrey & Buote 2008). Above this luminosity we extrapolated the XLF because no data are currently available and therefore the uncertainties are large. For the slope at the highest luminosities, we considered values in the range $\alpha_3 = [2, 6]$ and did not find any significant difference from the contours reported in Fig. 7.

For the HMXBs we used instead the luminosity function derived by Grimm et al. (2003). In particular, we used the cumulative form of it, corresponding to their Eq. (7):

$$N(> L_{38}) = 5.4\ \mathrm{SFR} \left(L_{38}^{-0.61} - 210^{-0.61}\right), \quad (3)$$

where the SFR is in units of $M_\odot$ yr^{-1}.

We then calculated the number of X-ray binaries with $L_{\rm X} > 10^{38}$ erg s^{-1} that we expect in each galaxy integrating the XLFs for a given SFR and $M_\star$. In Fig. 7 we show the contours corresponding to regions where we expect more than 0.1 (red), 1 (green), 5 (cyan), 10 (yellow) X-ray sources with $L_{\rm X} > 10^{38}$ erg s^{-1}. In reality these numbers have to be considered upper limits because we have not taken into account the limited Chandra spatial resolution that does not allow the detection of off-nuclear sources with small offsets (see Fig. 10 of Lehmer et al. 2006).

From Fig. 7 we find that all our ULX candidates are hosted in galaxies for which a large number of X-ray binaries is predicted. The dashed line in Fig. 7 is where we expect the same number of LMXBs and HMXBs with $L_{\rm X} > 10^{38}$ erg s^{-1}. This line clearly divides a region (below the line) where the XLF of LMXBs is dominating and therefore the contours are mainly defined by the $M_\star$ values, from a region (above the line) where the HMXBs are more numerous and the contours are determined by the level of the SFR. Our morphological classification is consistent with this picture: ETGs, characterized by a lower SFR and high stellar masses, are located in the bottom-right part of the plot, where the expected number of LMXBs is higher than the number of HMXBs. However, we note that there are suggestions in the literature that no ULX LMXBs may actually exist. Irwin et al. (2004) have shown that the number of ULXs detected in a sample of 28 ellipticals observed with Chandra is equal to the number of expected foreground/background objects. Additionally, these ULXs are uniformly distributed and do not follow the optical light of the galaxies. Irwin et al. (2004) also verified that the same statements can be made for the ULXs associated to early-type galaxies presented in Colbert & Ptak (2002).

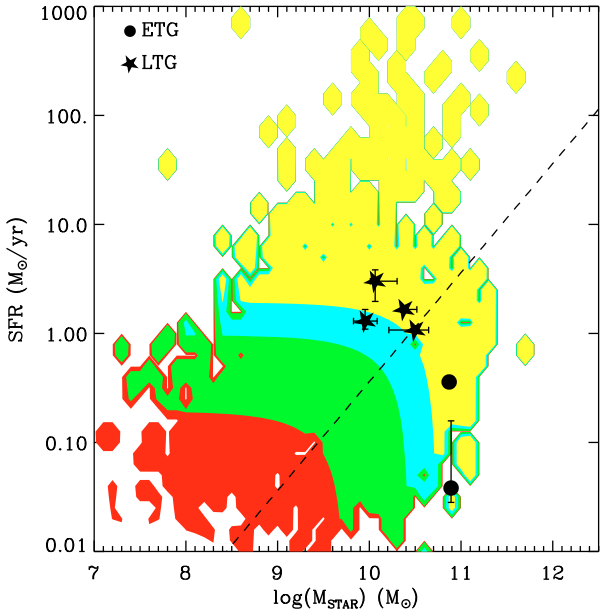

Fig. 7. SFR versus stellar masses of the galaxies in the comparison sample (see text). The contours correspond to the region where more than 0.1 (red), 1 (green), 5 (cyan), and 10 (yellow) X-ray off-nuclear sources per galaxy are expected. The symbols show the location in this plane of the host galaxies of the ULXs. For the source XID = 1151 the photometric coverage is limited to few bands and we cannot constrain its stellar mass. The symbols are the same as in Fig. 5. The dashed line is where we expect the same number of LMXBs and HMXBs with $L_{\rm X} > 10^{38}$ erg s^{-1}. Above this line the number of HMXBs is expected to be higher than that of LMXBs.

It would be interesting to repeat the same computation that generated Fig. 7 considering only X-ray binaries with $L_{\rm X} > 10^{39}$ erg s^{-1}, and therefore to be able to verify the hypothesis that ULXs are the high-luminosity tail of normal X-ray binaries. Unfortunately, this is not possible due to the poor knowledge of the high luminosity slope of the XLF for LMXBs and HMXBs.

4. Fraction of galaxies hosting a ULX

As already pointed out by Ptak & Colbert (2004), useful constraints on the nature of ULXs can be obtained deriving the fraction of galaxies that harbor a ULX as a function of the X-ray luminosity. For example, Körding et al. (2002) have compared the luminosity distribution of X-ray point sources in nearby galaxies with that predicted by X-ray population synthesis models

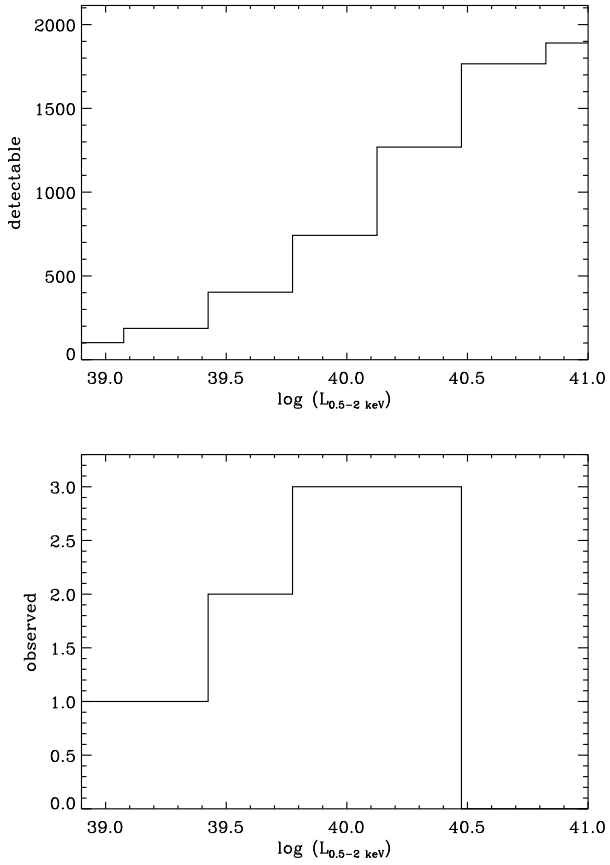

Fig. 8. *Top panel*: the number of galaxies for which we could detect an off-nuclear source of a given 0.5−2 keV luminosity $L_{0.5-2\ \mathrm{keV}}$ or higher. *Bottom panel*: the observed number of galaxies in each $L_{0.5-2\ \mathrm{keV}}$ bin hosting an ULX of luminosity $L_{0.5-2\ \mathrm{keV}}$ or higher.

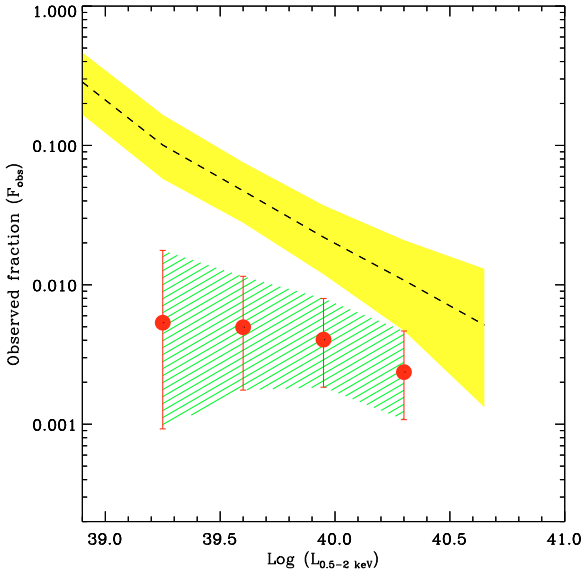

Fig. 9. Observed fraction of galaxies with an off-nuclear source with a luminosty of $L_{0.5-2\ \mathrm{keV}}$ or greater. The red points and associated 1σ confidence region are from our sample, while the dashed line and the 1σ confidence region were obtained by Lehmer et al. (2006) from the Chandra Deep Fields.

to check whether microblazars (microquasars with relativistically beamed jets pointing towards the observer) may represent an alternative to the intermediate mass black holes scenario for ULXs. In order to compute this fraction, we used the comparison sample selected in Sect. 3.2. We derived for each individual galaxy a 90% upper limit on its X-ray flux in the [0.5−2] keV band according to the procedure described in Sect. 6.5 of Puccetti et al. (2009), to which we refer the reader for details. The top panel of Fig. 8 shows the number of galaxies for which we could detect an off-nuclear source of 0.5−2 keV luminosity $L_{0.5-2\ \mathrm{keV}}$ or larger. The bottom panel of the same figure shows the observed number of galaxies in each $L_{0.5-2\ \mathrm{keV}}$ bin hosting an ULX of a luminosity $L_{0.5-2\ \mathrm{keV}}$ or larger. In order to derive the observed fraction of galaxies with an off-nuclear source, we divided the values of the histogram in the bottom panel by those in the top panel of Fig. 8. The result is shown in Fig. 9. The red points are the result of our analysis, and the dashed area is the 1σ confidence region computed with the prescriptions for small numbers statistic by Gehrels (1986). For comparison, we report in the same figure also the fractions obtained by Lehmer et al. (2006) from the Chandra Deep Fields (dashed line and 1σ confidence region). These fractions should be considered as lower limits due to the limited Chandra spatial resolution that does not allow the detection of off-nuclear sources with small offsets (see Fig. 10 of Lehmer et al. 2006). The agreement between our results and the CDFs points is reasonably good above $\log(L_{0.5-2\ \mathrm{keV}}) > 40$, although our point and the associated confidence contours are about a factor of two lower than, but consistent with, those derived by Lehmer et al. (2006).

In the lower luminosity bins, it seems that the two measures are discrepant; however, we do not consider this difference highly significant, since the measured fractions are consistent at the 2σ level. Also, at the faintest fluxes the differences between the two X-ray catalogs used is more severe. For these faint sources the positional uncertainties affecting our sample are larger than for the same sources detected in the longer Chandra exposures of the CDFs, and therefore we may be missing the faintest ULXs in the sample if their error box is consistent with the position of the nucleus. We also note that our selection criteria for off-nuclear sources reported in Sect. 2 are more conservative than those used by Lehmer et al. (2006). From Fig. 9 we found that ≈0.5% and ≈0.2% of the galaxies are hosting a ULX with $L_{0.5-2\ \mathrm{keV}} \gtrsim 3 \times 10^{39}$ and $L_{0.5-2\ \mathrm{keV}} \gtrsim 2 \times 10^{40}$ erg s^{-1}, respectively.

We now discuss the observed trend of the fraction of ULX as a function of their X-ray luminosities in the frame of the beaming model of King (2009). According to this model, ULX are stellar mass black holes accreting at a super-Eddington rate ($\dot{m} \equiv \dot{M}/\eta L_{\mathrm{Edd}}c^2 > 1$, for a typical radiative efficiency $\eta \sim 0.1$ and accretion rate $\dot{M}$). Matter accreting at these rates is easily blown away close to the inner edge of the accretion disk (Shakura & Sunyaev 1973); then, the radiative output from the resulting flow pattern is on the order of $L \approx L_{\mathrm{Edd}}(1 + \ln \dot{m})$, but emerges collimated by the central funnel with a beaming[6] factor $b \propto \dot{m}^{-2}$, so that an external observer who happens to have its line of sight within the beaming cone would infer a spherical luminosity: $L_{\mathrm{ULX}} \simeq 10^{39} m_7 (1 + \ln \dot{m})/b$ erg/s (where m_7 is the black hole mass in units of 7 solar masses; see King 2009 for further details). Thus, neglecting the weak logarithmic dependence on $\dot{m}$, this model directly links the observed luminosity of a ULX with its beaming factor b.

Let us now consider a population of ULX with a host galaxy space density (as a function of distance d): $n_{\mathrm{g}}(d)$ Mpc^{-3}.

[6] Note that here "beaming" simply means geometrical collimation, and not relativistic beaming.

The results of Lehmer et al. (2006) imply an almost linear decline of the cumulative number of ULX per galaxy with observed luminosity, $F_{\rm obs} \simeq F_0(L_{\rm ULX}/10^{39})^{-1}$, where $F_0 \simeq 0.1$ is the observed fraction of galaxies hosting a ULX with $L_{\rm ULX} > 10^{39}$. The differential fraction $\Phi_{\rm obs}$, i.e. the fraction of galaxies containing a ULX with luminosity $L_{\rm ULX}$ per unit logarithmic interval of luminosity can be derived by simply differentiating the above expression, to obtain $\Phi_{\rm obs} \equiv {\rm d}N/{\rm dLog}L_{\rm ULX} = F_0(L_{\rm ULX}/10^{39})^{-1} \approx F_0 b/m_7$, where the last approximate equality was derived neglecting the logarithmic dependence of $L_{\rm ULX}$ on b.

We now consider the application of this model to a multi-wavelength survey like COSMOS. We define the limiting flux of the survey in the X-ray band as $f_{\rm lim} = f_{-16} \times 10^{-16}$ erg s^{-1} cm^{-2}, so that an object of beaming factor b can be seen out to a distance of $d(b) = (10^{39} m_7/4\pi f_{\rm lim} b)^{1/2} \simeq 313 (b/m_7)^{-1/2} f_{-16}^{-1/2}$ Mpc, and express, in full generality, the number density of galaxies as a function of distance as $n_{\rm g}(d) = n_{\rm g}(d(b)) \equiv n_{\rm g,0}(b/m_7)^{\alpha}$, where $n_{\rm g,0}$ is the number density of possible host galaxies in the survey at the maximum distance where an un-beamed source ($b = 1$) can be seen. This expression is a very general form appropriate for power-law luminosity functions in Euclidean Universes and is adopted here for the sake of simplicity[7]; the exponent α depends both on the galaxy luminosity function slope and on the survey selection function and can in principle be derived empirically for any given survey: typically we have for flux-limited $\alpha > 0$, while volume limited ones have $\alpha \approx 0$. Given the observed cumulative fraction $F_{\rm obs}$[8], and the corresponding differential $\Phi_{\rm obs} = F_0 b/m_7$, one has to search through a space volume $V \sim 1/n_{\rm g}(d) F_0 (b/m_7)$ to find a ULX with beaming factor b (within a unit logarithmic interval of b). From this expression for the volume we derive

$$d(b) = 125 \left(A \frac{n_{\rm g,0}}{0.05} \frac{F_0}{0.1} \right)^{-1/3} \left(\frac{b}{m} \right)^{-(1+\alpha)/3} . \quad (4)$$

Thus, the minimum beaming factor (corresponding to the maximal luminosity) of a ULX in a survey of an area A (in units of square degrees) is given by

$$b_{\rm min} = 0.4^{\gamma} \left(f_{-16}^{\gamma/2} A^{-\gamma/3} \right) \left(\frac{n_{\rm g,0}}{0.05} \frac{F_0}{0.1} \right)^{-\gamma/3} m_7, \quad (5)$$

where $\gamma = \frac{6}{2\alpha - 1}$. The overall efficiency of finding ULX scales as $\ln L_{\rm ULX,max}$. We recall that $L_{\rm ULX}$ is the spherical luminosity that would be inferred by an external observer who happens to have his line of sight within the beaming cone. Applying this rough estimate with $\alpha = 1$, $m_7 = 1$, $n_{\rm g,0} = 0.05$, $F_0 = 0.1$ to the COSMOS survey ($f_{-16} \simeq 2$, $A = 0.9$), we obtain $b_{\rm min} \simeq 0.04$, $L_{\rm ULX,max} \simeq 2.5 \times 10^{40}$ in reasonable agreement with the present data. Interestingly, this also suggests that larger, but shallower, surveys could be more efficient in finding ULX (provided a similarly deep sample of host galaxies can be identified): the all sky eROSITA survey ($f_{-16} = 100$, $A = 4 \times 10^4$) could find a large number of ULX, including microblazars up to $b_{\rm min} = 2.6 \times 10^{-6}$, $L_{\rm ULX,max} \simeq 4.0 \times 10^{44}$.

[7] Although we applied a k-correction to the luminosity values in Eq. (1), we resolved to make the calculations in this paragraph under the assumption of a Euclidean Universe to simplify the derivation of Eq. (5).

[8] We assume in this calculation that the fraction of galaxies hosting a ULX does not change as a function of distance. This is an approximation, because the star formation rate varies with redshift, and therefore it is plausible that the fraction of galaxies hosting a ULX varies too.

Table 2. Properties of the host galaxies of ULXs in C-COSMOS.

XID[a]	i mag (AB)	$R_{\rm P}$[b] (arcsec)	z[c]	Class[d]	$\log(M_\star)$ ($M_\odot$)	SFR ($M_\odot$/yr)
1151[e]	15.62	19.89	0.094 p	ETG	...	...
1388	20.39	5.20	0.204 p	LTG	$10.1^{+0.2}_{-0.1}$	$3.0^{+0.8}_{-1.1}$
1870	18.40	9.21	0.072 s	LTG	$9.9^{+0.2}_{-0.1}$	$1.3^{+0.4}_{-0.2}$
2418	19.45	3.99	0.283 s	ETG	$10.9^{+0.1}_{-0.1}$	$0.3^{+0.1}_{-0.1}$
3441	18.19	5.50	0.133 s	LTG	$10.5^{+0.1}_{-0.3}$	$1.1^{+0.1}_{-0.1}$
11100	18.48	6.90	0.110 s	LTG	$10.4^{+0.1}_{-0.1}$	$1.7^{+0.1}_{-0.1}$
11938	18.94	2.53	0.221 p	ETG	$10.9^{+0.1}_{-0.1}$	$0.04^{+0.12}_{0.01}$

Notes. [(a)] ID of the Chandra source (Elvis et al. 2009). [(b)] Petrosian radius of the host galaxy Petrosian (1976). [(c)] Redshift of the host galaxy: "s" for spectroscopic and "p" for photometric redshifts. [(d)] Morphological classification of the ULX host galaxy: early type galaxy (ETG) or late type galaxy (LTG). [(e)] The photometric coverage is limited to few bands and we cannot constrain its $M_\star$ or SFR.

5. Conclusions

We presented a sample of ultraluminous X-ray sources (ULXs) selected from the Chandra survey in the COSMOS area (C-COSMOS). From 1761 X-ray sources detected with a maximum likelihood threshold of detml = 10.8 in at least one detection band, we selected 7 ULX candidates covering the redshift range $z = 0.072$–0.283.

Taking advantage of the excellent ancillary data available in the COSMOS field, we studied the properties of their host galaxies. From a detailed morphological analysis of the ACS images and rest-frame colors, we found that ULXs are hosted both in late and in early type galaxies, with a slight preference for the former.

From the multi-band photometry and from the optical spectral lines, we measured stellar masses and star formation rates for the host galaxies. Using literature X-ray luminosity functions for HMXBs and LMXBs, we defined probability areas for having detectable off-nuclear sources in the plane SFR versus $M_\star$. All our ULXs candidates are hosted in galaxies for which we expect a large number of X-ray binaries with $L > 10^{38}$ erg s^{-1}.

The presence of IMBHs ($\sim 10^2$–$10^5 M_\odot$) in some of our ULXs cannot be excluded with the current data. The best candidates for this new class of accreting black holes are the ULXs hosted in early type galaxies (therefore not associated with recent star formation activity) and with X-ray luminosity above 10^{41} erg s^{-1} that can be difficult to explain with high-mass stellar black holes. The objects that satisfy these criteria from our sample are XID = 2418 and 11938. Longer X-ray exposures could give us more insights into the real nature of these sources from a detailed study of the X-ray spectrum. Similarly, we cannot set constraints on the recoiling black-hole nature of our sources with the current data, but it is worth mentioning that recent predictions by Volonteri & Madau (2008) expect at most one of these objects in the C-COSMOS survey, assuming the most favorable scenario (spinning black holes, no bulge in the host galaxy, long active phase).

Finally, we derived the fraction of galaxies hosting a ULX as a function of the X-ray luminosity. We found that ≈0.5% and ≈0.2% of the galaxies are hosting a ULX with $L_{0.5-2\ {\rm keV}} \gtrsim 3 \times 10^{39}$ and $L_{0.5-2\ {\rm keV}} \gtrsim 2 \times 10^{40}$ erg s^{-1}. This agrees reasonably well with the observed fraction derived in the Chandra Deep Fields by Lehmer et al. (2006) above $\log(L_{0.5-2\ {\rm keV}} > 40$ erg s^{-1}.

A possible discrepancy in the lower luminosity bins can be likely attributed to the differences in the limiting fluxes of the two catalogs and, therefore, to the different positional uncertainties affecting faint X-ray sources.

Acknowledgements. This work is based on observations made with ESO Telescopes at the La Silla or Paranal Observatories under programme ID 175.A-0839. We are grateful to the referee for detailed and extremely useful comments that improved the quality of the paper. We thank Piero Rosati and Bret Lehmer for useful scientific discussions. We are grateful to Bret Lehmer for providing the data points of the CDFs used in Fig. 9. This work has been supported in part by the grants: ASI/COFIS/WP3110 I/026/07/0, ASI/INAF I/023/05/0, ASI I/088/06/0, PRIN/MIUR 2006-02-5203.

References

Begelman, M. C. 2002, ApJ, 568, 97
Bruzual, G., & Charlot, S. 2003, MNRAS, 344, 1000
Bolzonella, M., Kovac, K., Pozzetti, L., et al. 2009, A&A, submitted [arXiv:0907.0013]
Capak, P., Aussel, H., Ajiki, M., et al. 2007, ApJS, 172, 99
Colbert, E. J. M., & Mushotzky, R. F. 1999, ApJ, 519, 89
Colbert, E. J. M., & Ptak, A. F. 2002, ApJS, 143, 25
Damiani, F. Maggio, A., Micela, G., & Sciortino, S. 1997, ApJ, 483, 350
Elvis, M., Civano, F., Vignali, C., et al. 2009, ApJS, 184, 158
Fabbiano, G. 1989, ARA&A, 27, 87
Gehrels, N. 1986, ApJ, 303, 336
Gilfanov, M. 2004, MNRAS, 349, 146
Grimm, H.-J., Gilfanov, M., & Sunyaev, R. 2003, MNRAS, 339, 793
Hopman, C., Portegies Zwart, S. F., & Alexander, T. 2004, ApJ, 604, L101
Humphrey, P. J., & Buote, D. A. 2008, ApJ, 689, 983
Ilbert, O. Capak, P., Salvato, M., et al. 2009, ApJ, 690, 1236
Irwin, J. A. Bregman, J. N., & Athey, A. E. 2004, ApJ, 601, L143
Kennicutt, R. C. Jr. 1998, ARA&A, 36,189
Kim, D.-W., & Fabbiano, G. 2004, ApJ, 611, 846
King, A. R. 2002, MNRAS, 335, L13
King, A. R., 2009, MNRAS, 393, L41
Koekemoer, A. M., Aussel, H., Calzetti, D., et al. 2007, ApJS 172, 196
Körding, E., Falke, H., & Markoff, S. 2002, A&A, 382, L13
Lehmer, B. D., Brandt, W. N., Hornschemeier, A. E., et al. 2006, AJ, 131, 2394
Lilly, S., Le Fèvre, O., Renzini, A., et al. 2007, ApJS, 172, 70
Lilly, S. Le Brun, V., Maier, C., et al. 2009, ApJS, 184, 218
Liu, Q. Z., & Mirabel, I. F. 2005, A&A, 429, 1125
Makishima, K., Kubota, A., Mizuno, T., et al. 2000, ApJ, 535, 632
Maier, C. Lilly, S. J., Carollo, C. M., Stockton, A., & Brodwin, M. 2005, ApJ, 634, 849
Mignoli, M. Zamorani, G., Scodeggio, M., et al. 2009, A&A, 493, 39
Miller, M. C., & Colbert, E.J. M. 2004, Int. J. Mod. Phys., D13, 1
Moustakas, J., Kennicutt, R. C. Jr., & Tremonti, C. 2006, ApJ, 642, 775
Ptak, A., & Colbert, E. 2004, ApJ, 606, 291
Petrosian, V. 1976, ApJ, 209, L1
Puccetti, S. Vignali, C., Cappelluti, N., et al. 2009, ApJS, 185, 586
O'Donnell, J. E. 1994, ApJ, 422, 158
Roberts, T. P., Warwick, R. S., Ward, M. J., & Goad, M. R. 2004, MNRAS, 349, 1193
Shakura N., & Sunyaev, R., 1973, A&A, 24, 337
Salvato, M., Hasinger, G., Ilbert, O., et al. 2009, ApJ, 690, 1250
Scarlata, C., Carollo, C. M., Lilly, S., et al. 2007, ApJS, 172, 406
Seaton, M. J. 1979, MNRAS, 187, 76P
Swartz, D. A., Ghosh, K. K., Tennant, A. F., & Wu, K. 2004, ApJS, 154, 519
Volonteri, M., & Madau, P., 2008, ApJ, 687, L57